Electronic Supplementary Information

Probing liquid behaviour by helium atom scattering: surface structure and phase transitions of an ionic liquid on Au(111)

Eliza M. McIntosh, John Ellis, Andrew P. Jardine, Peter Licence, Robert G. Jones and William Allison

Details of ionic liquid evaporator used to deposit $[C_2C_1Im][Tf_2N]$ onto the Au(111) surface

To collimate the ionic liquid vapour during deposition onto the crystal surface and avoid contamination of the scattering chamber a custom evaporator was designed and built using components manufactured in the Cavendish Laboratory workshops and vacuum parts from external suppliers. The evaporator was mounted externally to the scattering chamber of the Cambridge helium spin-echo (HeSE) spectrometer to maintain sufficient distance between the evaporator and crystal to form a well collimated beam. A gate valve, which could be shut when heating the evaporator and if problems arose during deposition, separated the evaporator from the chamber.

Figure S1a shows the evaporator insert, which comprises a Pyrex crucible in a copper oven to ensure even heating of the liquid, with heating provided by a naked car headlamp filament. K-type thermocouples, with the ends trapped against the copper oven by screws, are used to monitor the temperature of the oven. The Pyrex crucible holds approximately 1 ml of liquid without spillage at the 45^0 down angle at which the evaporator had to fit onto the HeSE apparatus due to pre-existing space constraints. The capillary tube entrance to the Pyrex crucible is of inner diameter 3.3 mm and forms the first aperture to collimate the beam. Glass wool is packed around the Pyrex crucible to ensure a snug fit in the copper oven.

The full evaporator assembly is shown in Figure S1b. The evaporator insert is connected to the rest of the evaporator assembly by a piece of studding, and ceramic balls held in place by Beryllium Copper braces are used to locate the evaporator insert in the stainless steel tubing of the vacuum system such that the central tube is located centrally in the evaporator assembly to an accuracy of ± 1 mm. A linear feed-through was fitted to the small bore side of the four way cross opposite the pump and ion gauge to enable the use of a flag with an additional drip tray.

The dimensions of the second aperture used to collimate the beam, positioned 270 mm from the first, were calculated using ray diagrams, requiring the incident flux to dose a region of the crystal of 8 mm diameter. The second aperture was cut into a stainless steel plug at the bottom end of a stainless steel pipe secured to a blank Copper gasket by Swagelok fittings, to additionally provide differential pumping between the upper and lower parts of the evaporator. The collimation of the evaporator was tested before installation on the HeSE spectrometer by evaporating sufficient liquid onto a windowed flange to verify visually that the beam was focussed to the expected dimensions.

The bottom end of the evaporator assembly, below the collimator and drip tray, connects to the HeSE spectrometer by a port aligner to allow alignment of the evaporator with the crystal. The evaporator was installed on the Cambridge HeSE spectrometer and the arm baked to achieve a base pressure P_{evap} $< 2 \times 10^{-8}$ mbar , with a windowed flange at the top end instead of the evaporator insert. After baking, the gate valve was then opened and the evaporator aligned by adjusting the port aligner while sighting the crystal through a small optical telescope. Once the evaporator had been aligned it was clamped in place using a support bracket, the evaporator insert replaced, and the arm baked first with the evaporator insert but no ionic liquid sample to recover the base pressure, and then for a short time with the ionic liquid sample added to the Pyrex vial.

A filament current of 5.5 A (10.6 V) was used to reach a temperature of ~150^0C in about 30 minutes. A further ~30 minutes at a constant temperature of 150^0C with a lower filament current of 3.9 A (4.5 V) were then needed for a significant pressure rise to be measured, indicating that evaporation had started. During deposition the pressure and temperature in the evaporator were monitored, and to dose $[C_2C_1Im][Tf_2N]$ onto the crystal the gate valve and then the flag were opened.

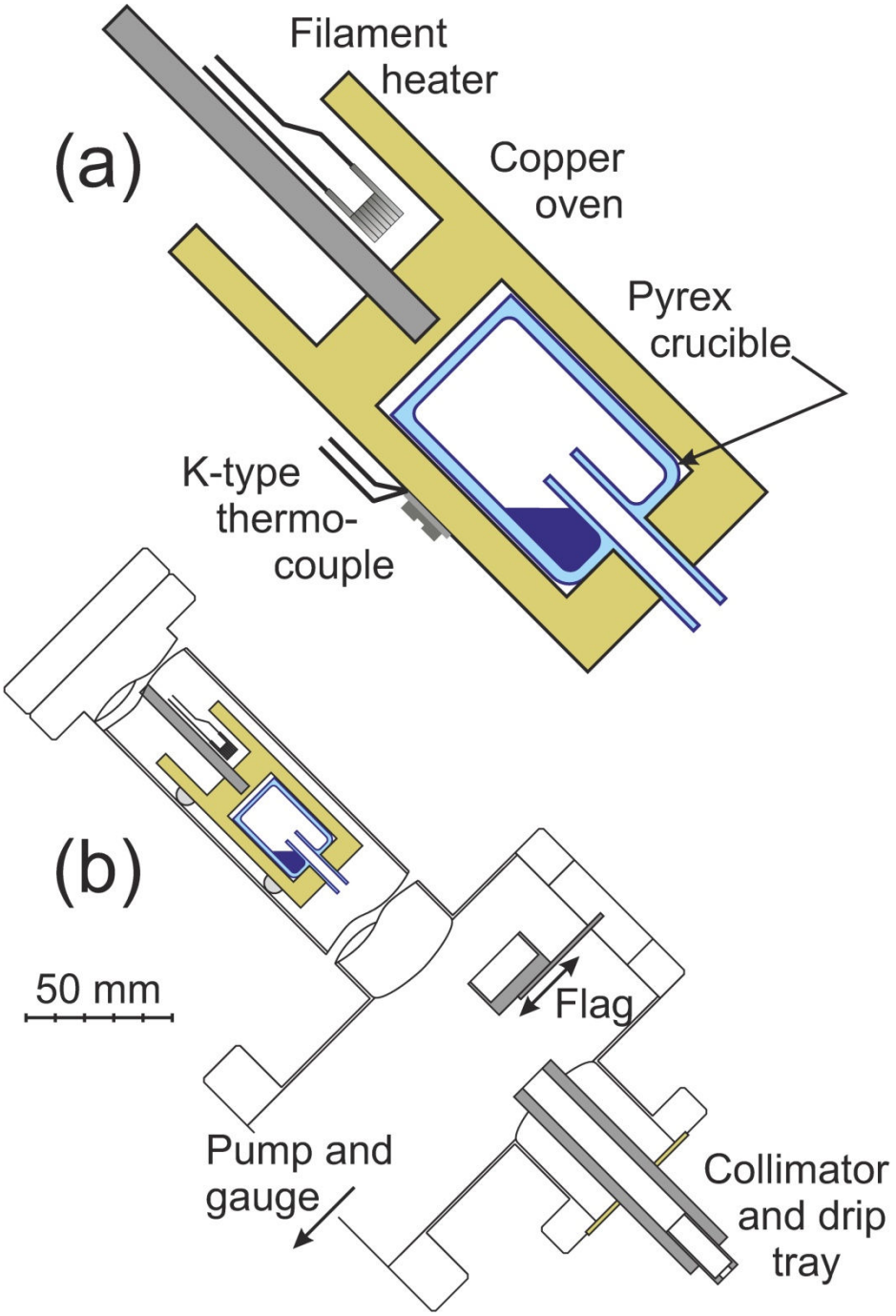

Fig. S1 Cross-section through the ionic liquid evaporator. a) evaporator insert and b) the entire evaporator assembly. The evaporator assembly is joined to the chamber at the bottom end via a port aligner and gate valve. After alignment, the upper end of the evaporator assembly is secured in position with a bracket. The distance from the bottom of the evaporator to the crystal is 270 mm.

Figure S2 shows photographs of (a) the evaporator insert and (b) the entire evaporator assembly mounted on the Cambridge HeSE spectrometer. In figure S2a the copper oven is discoloured due to a reaction between the ionic liquid vapour and the copper, emphasising the need for the Pyrex crucible to prevent the copper oven coming into contact with the liquid.

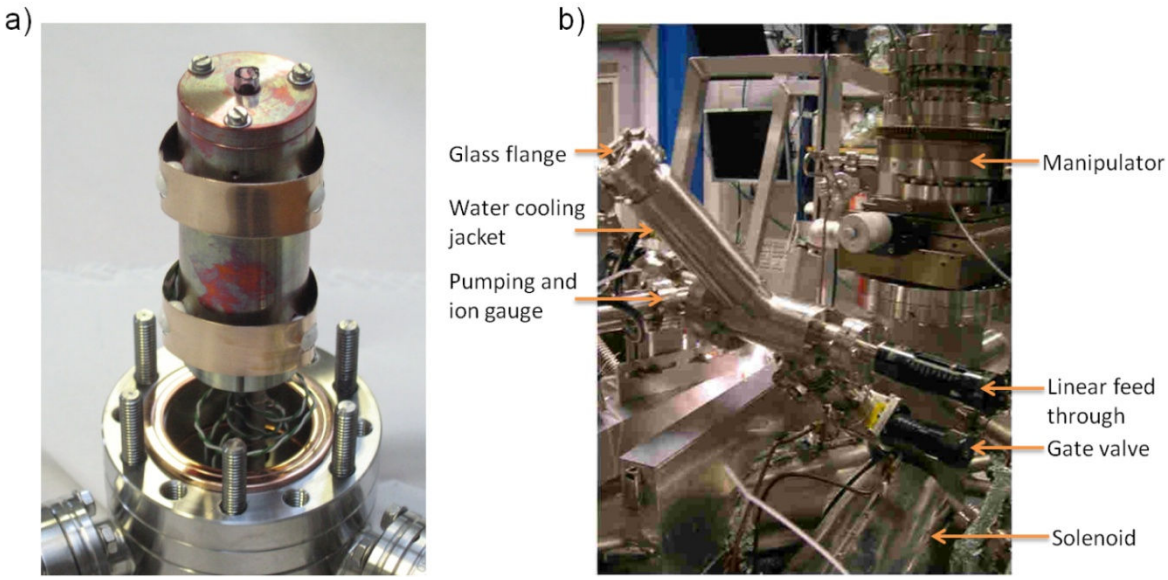

Fig. S2 The ionic liquid evaporator used for the experiments described in the main article. (a) Evaporator insert, as shown in cross-section in Figure S1a. The copper oven has become discoloured by exposure to $[C_2C_1Im][Tf_2N]$ vapour. (b) Evaporator assembly mounted on the HeSE spectrometer. For experiments the glass flange on the end was replaced with the evaporator insert, as described in the text. The HeSE manipulator and a spin-precession solenoid are labelled, along with some external components of the evaporator assembly.

Temperature Programmed Desorption (TPD) measurements of multilayer desorption

Figure S3 shows TPD results for the desorption of a thick film of $[C_2C_1Im][Tf_2N]$ from Au(111), following adsorption at T_s = 200 K. The top panel shows the mass spectrometer count rate at m/z = 111 ($[C_2C_1Im]^+$) and the bottom panel the specularly reflected intensity of helium from the surface, which was measured simultaneously. Two main peaks are seen in the mass spectrometer counts: a multilayer peak just below 400 K and a single layer peak around 500 K. The positions of these peaks are in agreement with the recent TPD results of Hessey and Jones for the same system[1]. There is no change in the specularly reflected intensity of helium during desorption of the 400K peak, indicating that the morphology and order in the surface layer remains unchanged until approximately 480K. The observation supports the assignment of the desorption peak at 400K to multi-layer desorption. Similarly, the distinct changes in reflectivity above 480K are indicative of the high reflectivity of the underlying gold surface and suggest strongly that the high temperature peak corresponds to monolayer desorption.

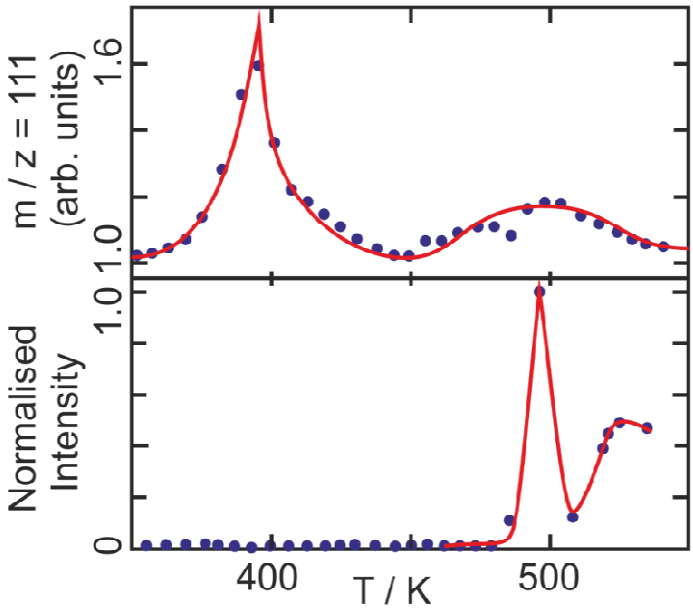

Fig. S3 TPD results for the desorption of $[C_2C_1Im][Tf_2N]$ from Au(111). Top: mass spectrometer count rate at m/z = 111; Bottom: specularly reflected intensity of helium normalised to the maximum count rate. Measured data points are shown as filled circles, the lines are a guide to the eye.

Calibration of dose of $[C_2C_1Im][Tf_2N]$ for uptake curves

In this section, we briefly explain how the dose axis of uptake curves (Figure 2 of the main paper and Figure S4) was calibrated.

Although the temperature of the evaporator was held constant during deposition of $[C_2C_1Im][Tf_2N]$ the evaporation rate varied slightly during the uptake due to instabilities in the evaporator. The vapour pressure in the evaporator arm was measured and found to be linearly proportional to the flux of $[C_2C_1Im][Tf_2N]$ at the crystal surface. For example for the blue curve in Figure 2a, the pressure measured in the evaporator, $P_{evap,}$ was alternately higher (~ 2 x 10^{-6} mbar) and lower (~ 5 x 10^{-7} mbar). The dose axis was therefore calibrated in mbar.s using the measured evaporator pressures, although, as the pressure measured in the evaporator is not equal to the pressure at the crystal surface, this gives only a relative measure of the dose of $[C_2C_1Im][Tf_2N]$.

Reflectivity during uptake at 250 K and 320 K

Figure S4 shows the specularly reflected intensity of helium as a function of dose of $[C_2C_1Im][Tf_2N]$ at surface temperatures of 200 K (blue, as in Figure 2a of the main article), 250 K (red) and 320 K (green). Only data at high dose is shown, to facilitate comparison of the shape of the uptake curves in this region. All data is shown on an arbitrary intensity scale and the curves are offset for clarity.

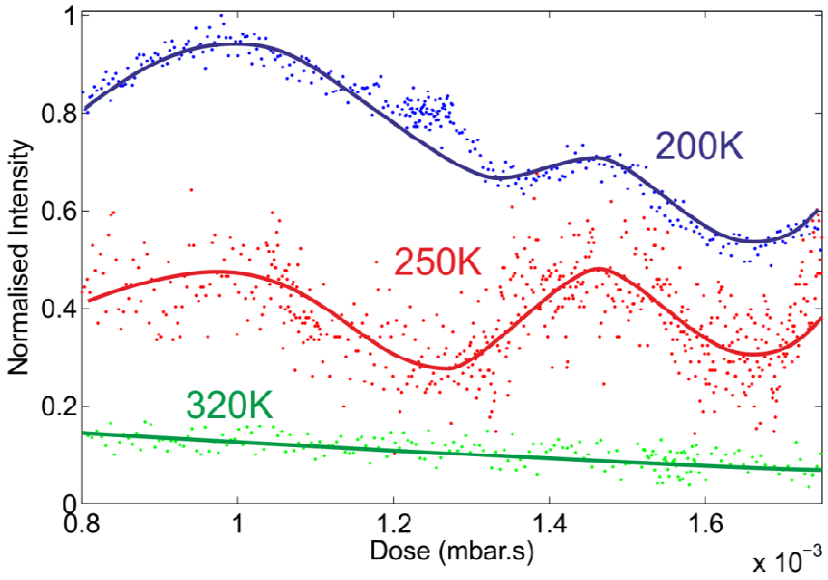

Fig. S4 Uptake curves showing the variation of the specularly reflected intensity of helium-3during exposure to $[C_2C_1Im][Tf_2N]$. The curves are scaled vertically and offset for clarity to allow the shape to be compared. The temperatures on the figure give the temperature at which the substrate was held during the uptake. At T_s = 200 K and 250 K oscillations are seen in the uptake curves corresponding to periodic ordering and disordering of the substrate. Above the melting temperature at T_s = 320 K no oscillations are seen. As discussed in the main article and above in the ESI, the *x*-axis is calibrated in units of mbar.s to account for variations in the pressure in the evaporator during the dose.

It is clear that while oscillations exist in the uptake curves at both T_s = 200 K and T_s = 250 K, the oscillations are less pronounced at T_s = 250 K and are not visible in the uptake curve at T_s = 320 K, supporting the assertion made in the main article.

Diffraction scans of the clean Au(111) surface

Figure S5 shows helium diffraction scans of the clean Au(111) surface along the two high symmetry directions, <1 1 0> and <1 1 2 >. The positions and relative intensities of the peaks confirm the presence of the (23 × √3) reconstruction of the clean Au(111) surface[2, 3]. In both directions the specular peak has been removed for clarity as it has a relative intensity of 200 x the maximum intensity shown in the Figure.

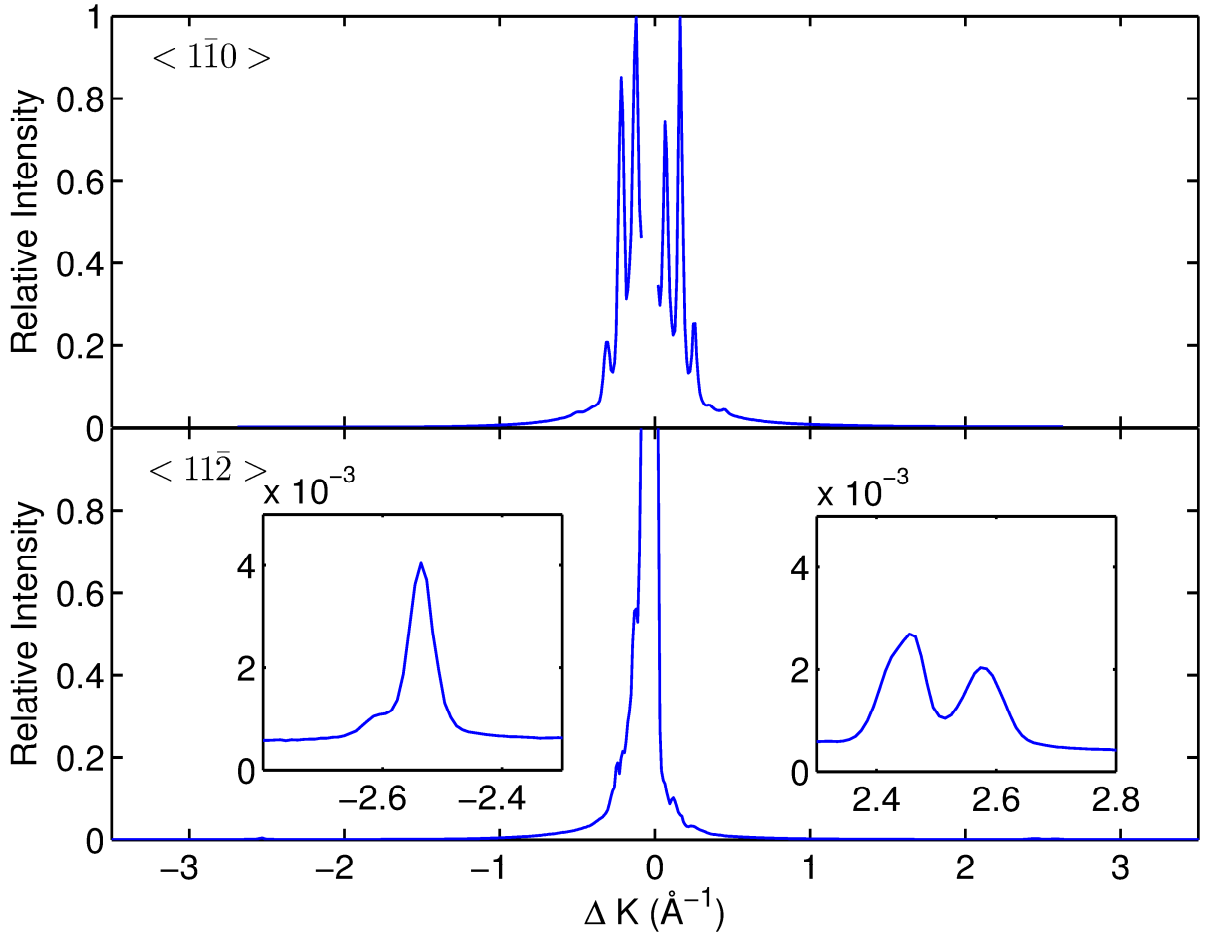

Fig. S5 Helium-3 diffraction scans of the clean Au(111) surface along <1 $\bar{1}$ 0> (top) and <11 $\bar{2}$ > (bottom) at T_s = 200 K. Insets show details of the diffraction peaks $\Delta\mathbf{K}$ ~ 2.5 Å^{-1} along <11 $\bar{2}$ >. The *y*-axis allows the relative intensity of features in the diffraction scans to be compared; a relative intensity of 1 corresponds to 1/200 of the intensity of the specular peak (at $\Delta\mathbf{K}$ = 0 Å^{-1}).

Estimation of domain size from width of elastic peaks in diffraction patterns

The width of the elastic diffraction peaks in Figure 4 of the main article was used to provide an estimate of the domain size of $[C_2C_1Im][Tf_2N]$ on the Au(111) surface. More formally, following the treatment of Comsa[4], the angular full width half-maximum (FWHM), $\Delta\theta_f$, of a diffraction peak has contributions from the energy spread of the helium beam, $\Delta_E\theta_f$, the angular resolution of the apparatus, $\Delta_\theta\theta_f$, and the disorder on the surface, $\Delta_d\theta_f$, and can be expressed in terms of these contributions using the convolution theorem as[4]:

$$(\Delta\theta_f)^2 = (\Delta_E\theta_f)^2 + (\Delta_\theta\theta_f)^2 + (\Delta_d\theta_f)^2 \qquad \text{(equation S1)}$$

The angular resolution of the Cambridge HeSE spectrometer $\Delta_\theta\theta_f \sim 0.1°$, and the energy profile of the incident beam was measured, indicating that the beam of energy, E = 8.0 meV used for the experiments reported had a FWHM, ΔE, of 0.25 meV, allowing the mean angular width due to disorder, $\Delta_E\theta_f$, to also be determined using[4]

$$\Delta_E\theta_f \approx \frac{|\sin(\theta_i) - \sin(\theta_f)|(\Delta E/E)}{\cos(\theta_f)} \qquad \text{(equation S2)}$$

Therefore, from the measured total angular width of an elastic peak in a diffraction scan, $\Delta\theta_f$, the disorder on the surface, $\Delta_d\theta_f$, can be found using equation S1. From $\Delta_d\theta_f$ the domain size on the surface, l_d, can then be estimated from[5]

$$l_d = \frac{2\pi}{k_i\Delta_d\theta_f|\cos(\theta_f)|}, \qquad \text{(equation S3)}$$

where k_i is the momentum carried by the incident helium beam in units of $Å^{-1}$.

For the elastic diffraction peaks in Figure 4 of the main article, if instrumental effects are ignored and the measured angular width of the diffraction peaks, $\Delta\theta_f$, is used instead of $\Delta_d\theta_f$ in equation S3, a lower bound on the domain size at the surface of multilayers of $[C_2C_1Im][Tf_2N]$ in the solid phase of 120 Å is obtained. If instrumental effects are also considered, the angular width expected from the angular resolution and the angular broadening at the position of the diffraction peaks from the energy spread of the beam together give a broadening comparable to the experimentally observed peak widths, leaving an extremely small contribution to the broadening from $\Delta_d\theta_f$ and indicating that the domain size on the surface is in fact considerably larger than 120 Å with long range order at the surface.

Determination of overlayer structure

Figure S3 below is a reciprocal space diagram illustrating the positions of the observed diffraction peaks along the <1 1 0> and <11 2 > type directions shown in Figure 4 of the main article. ***a**** is the primitive reciprocal space mesh of gold where $\boldsymbol{a}_1^*$ and $\boldsymbol{a}_2^*$ are the primitive reciprocal space translation vectors for the unreconstructed gold surface, $|\boldsymbol{a}_1^*|=|\boldsymbol{a}_2^*|$ and $|\boldsymbol{a}_1^*| = 2\pi/a = 2.178$Å, where a (=2.885 Å) is the surface lattice constant for Au(111) .

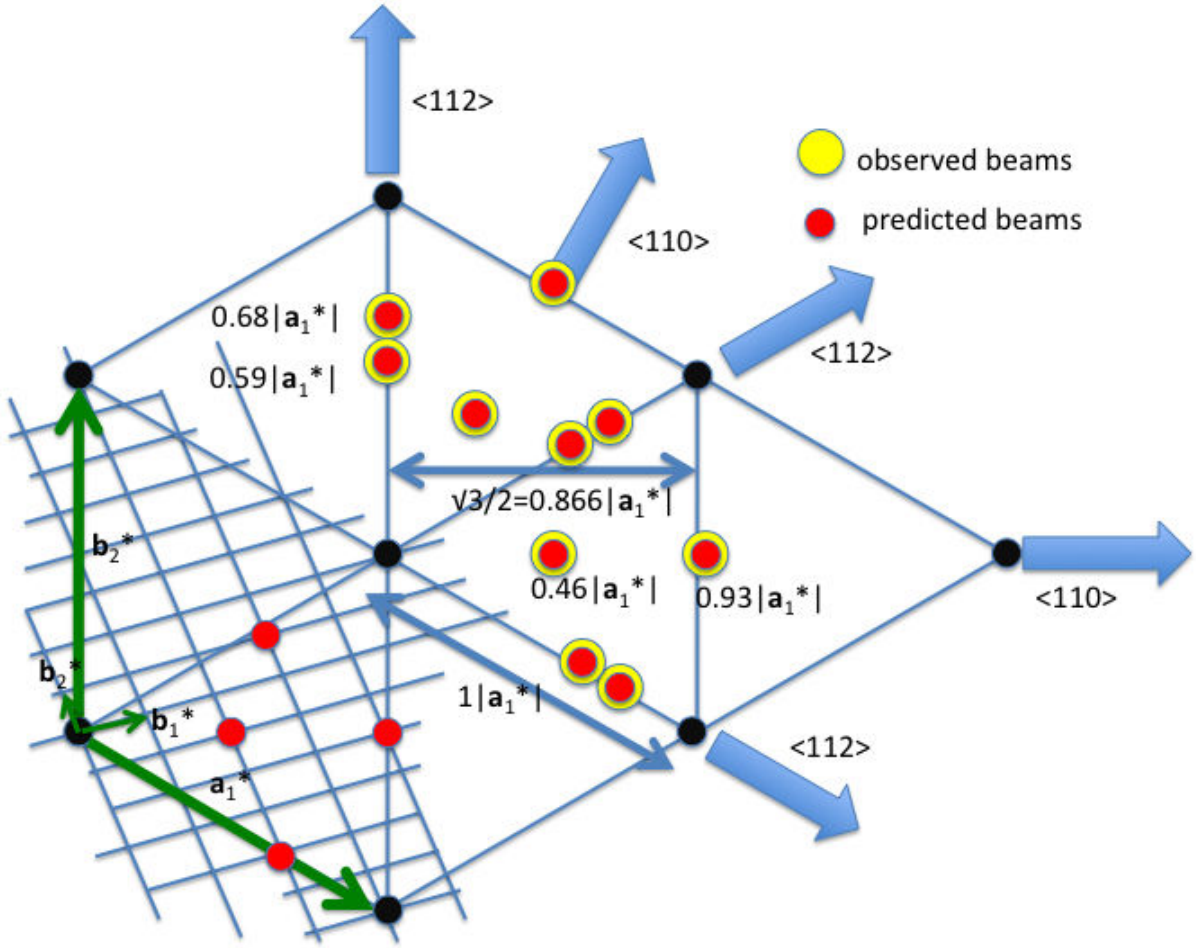

Fig. S3 Reciprocal space diagram showing the integral order beams for the bulk terminated Au(111) a net (vectors $\boldsymbol{a}_1$ and $\boldsymbol{a}_2$) and equivalent <1 $\overline{1}$ 0> and <11 $\overline{2}$ > directions. Experimentally determined diffraction beams are shown as yellow circles along several equivalent directions, marked with their position in units of $|\boldsymbol{a}_1|$. In the lower left hand corner the reciprocal space net of the (3 2, -6 8) structure (one of six orientations) is shown, where beams would occur at each vertex of the net. Red circles mark where predicted beams are observed experimentally for the just one orientation (lower left) and for all orientations (upper right).

In the <1 $\overline{1}$ 0> type direction two peaks were observed at 1.00 Å^{-1} and 2.02 Å^{-1} which corresponds to $0.46|\underline{\boldsymbol{a}}_1^*|$ and $0.93\ |\underline{\boldsymbol{a}}_1^*|$. These correspond (within experimental error of ±0.05) to $\sqrt{3}/4|\underline{\boldsymbol{a}}_1^*|$ and $2\sqrt{3}/4|\underline{\boldsymbol{a}}_1^*|$, i.e. ¼ order positions between substrate integral order diffraction beams in this direction.
In the <11 $\overline{2}$ > directions three peaks were observed at 1.275 Å^{-1}, 1.476 Å^{-1}, and 2.498 Å^{-1} which correspond to $0.59|\underline{\boldsymbol{a}}_1^*|$, $0.68|\underline{\boldsymbol{a}}_1^*|$ and $1.15|\underline{\boldsymbol{a}}_1^*|$. The first could correspond to 4/7th (0.571), 5/9th (0.55) or 6/10th (0.6) of the distance between integral order beam, while the second corresponds to 2/3rd of the distance between the integral order diffraction beams in this direction. The third is double the value of the first (not shown in Figure S3).

Many models were considered, but it was thought that a plane within the bulk crystal structure of the ionic liquid, closely matching the Au(111) unreconstructed surface, would be the most likely to explain the observed diffraction pattern. We used the *ab* plane of solid $[C_2C_1Im][Tf_2N]$ to search for coincidence, or near coincidence nets. The *ab* plane could form a coincident net with Au(111) to form a (3x√37)Rect structure, but while this would give 1/3 and /1/7th order beams along the <11 $\bar{2}$ > directions (which matches experiment) no match is found for the beams in the <1 $\bar{1}$ 0> direction.

A possible structure that gives beams in the correct positions has the matrix notation $\boldsymbol{M}$ = (3 2, -6 8). Figure S4 illustrates the relation between the proposed structure for adsorbed layers of $[C_2C_1Im][Tf_2N]$ on the Au(111) surface described by the matrix notation $\boldsymbol{M}$ = (3 2, -6 8). Figure S4a shows the *ab* plane of $[C_2C_1Im][Tf_2N]$ with the positive and negative ions identified as red and blue circles respectively. The parallelogram, outlined in yellow, after slight distortion and expansion matches the unit mesh (yellow, vectors $\boldsymbol{b}_1$ and $\boldsymbol{b}_2$) shown in Figure S4b which has the matrix notation (3 2, -6 8). The area per ion pair in the bulk *ab* structure is 79.87 Å^2 while the area per ion pair in the (3 2, -6 8) structure is slightly greater at 86.49Å^2. We do not know the arrangement of the ions within the (3 2, -6 8) unit mesh but speculate that they will be similar to the positions within the solid *ab* layer *i.e.* with alternate positive and negative ions aligned in rows parallel to the close packed direction of the Au(111) with the imidazolium ions parallel to the surface. . Using the *b* net shown in Figure S4, the reciprocal space matrix is calculated as (4/18 1/6, -1/18 1/12). This is shown in the bottom left part of Figure S3. There are six possible rotational orientations of this net on the Au(111) surface, such that all beams along a particular direction will occur in all equivalent directions. The vast majority of the beams do not lie along the crystal directions measured experimentally. The observed diffraction beams along <1 $\bar{1}$ 0> type directions are reproduced at ¼ and ½ the spacing to the next integral order position. Along the <11 $\bar{2}$ > directions one beam is accurately reproduced at 2/3 of the spacing to the next integral order. Another beam lies just off the <11 $\bar{2}$ > direction but at the correct position for the observed 0.585|$\boldsymbol{a}_1^*$| beam. A mirror image of this beam will occur on the other side of the <11 $\bar{2}$ > direction due to the mirror image domain of the *b* net on the gold surface, and hence the two of them would be recorded as a beam along <11 $\bar{2}$ >. A beam at 1/3rd along the <11 $\bar{2}$ > direction is also predicted but not seen experimentally.

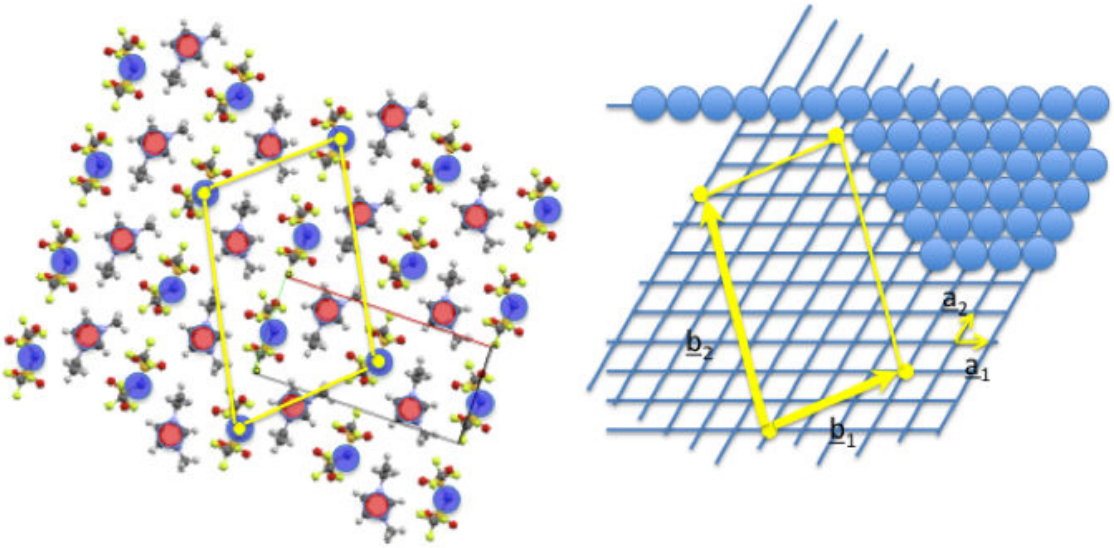

(a) (b)

Fig. S4 (a) *ab* plane of solid $[C_2C_1Im][Tf_2N]$ with anions (blue circles) and cations (red circles) identified. The yellow parallelogram (not a unit mesh) shows a repeating unit containing three ion pairs. (b) diagram of the bulk terminated Au(111) showing the substrate unit mesh, $\mathbf{a}_1$ and $\mathbf{a}_2$, and the adlayer mesh, $\mathbf{b}_1$ and $\mathbf{b}_2$.

1. S. Hessey and R. G. Jones, *Chemical Science*, 2012, **4**, 2519-2529.
2. E. M. McIntosh, P. R. Kole, M. El-Batanouny, D. Chisnall, J. Ellis and W. Allison, *Physical Review Letters*, 2013, **110**, 086103.
3. U. Harten, A. M. Lahee, J. P. Toennies and C. Woell, *Physical Review Letters*, 1985, **54**, 2619-2622.

4. G. Comsa, *Surface Science*, 1979, **81**, 57-68.
5. N. Camillone III, C. E. D. Chidsey, G.-Y. Liu, T. M. Putvinski and G. Scoles, *Journal of Chemical Physics*, 1991, **94**, 8493-8502.